CRISPR-Cas immunity repressed by a biofilm-activating pathway in *Pseudomonas aeruginosa*

Adair L. Borges#, Bardo Castro#, Sutharsan Govindarajan, Tina Solvik, Veronica Escalante, Joseph Bondy-Denomy*

Department of Microbiology & Immunology and the Quantitative Biosciences Institute, University of California, San Francisco, San Francisco, CA 94158

#Equal contribution

*Corresponding author: joseph.bondy-denomy@ucsf.edu

CRISPR-Cas systems are adaptive immune systems that protect bacteria from bacteriophage (phage) infection. To provide immunity, RNA-guided protein surveillance complexes recognize foreign nucleic acids, triggering their destruction by Cas nucleases. While the essential requirements for immune activity are well understood, the physiological cues that regulate CRISPR-Cas expression are not. Here, a forward genetic screen identifies a two-component system (KinB/AlgB), previously characterized in regulating *Pseudomonas aeruginosa* virulence and biofilm establishment, as a regulator of the biogenesis of the Type I-F CRISPR-Cas surveillance complex. Downstream of the KinB/AlgB system, activators of biofilm production AlgU (a σ^E orthologue) and AlgR, act as repressors of CRISPR-Cas surveillance complex expression during planktonic and surface-associated growth. AmrZ, another biofilm activator, functions as a surface-specific repressor of CRISPR-Cas activity. *Pseudomonas* phages and plasmids have taken advantage of this regulatory scheme, and carry hijacked homologs of AmrZ, which are functional CRISPR-Cas repressors. This suggests that while CRISPR-Cas regulation may be important to limit self-toxicity, endogenous repressive pathways represent a vulnerability for parasite manipulation.

Clustered regularly interspaced short palindromic repeats (CRISPR) and CRISPR-associated (cas) genes are RNA-guided nucleases found in nearly half of all bacteria[1]. CRISPR-Cas systems are mechanistically diverse, with six distinct types (I-VI) identified, based on signature genes, mechanisms of action, and the type of nucleic acid target[1].

35 Our strong understanding of the basic components to enable sequence specific DNA
36 and RNA cleavage have enabled functional transplantation into heterologous bacterial[2,3]
37 and eukaryotic[4,5] hosts. Given that many Cas proteins encode nucleases[6] the fine-tuned
38 regulation of these systems to avoid toxicity is likely a key factor to enable safe retention
39 of a CRISPR-Cas immune system[7]. Multiple signals have been shown to activate
40 CRISPR-Cas function in diverse organisms, such as quorum sensing[8,9], temperature[10],
41 membrane stress[11,12], altered host metabolite levels[13,14], and phage infection[15-18].
42 However, relatively little is known regarding the factors and/or signals that serve to
43 temper CRISPR-Cas activity and mitigate the risk of acquiring and expressing a
44 nucleolytic immune system.
45
46 Type I CRISPR-Cas systems are comprised of a multi-subunit RNA-guided surveillance
47 complex, a trans-acting nuclease (Cas3)[19-21], and proteins dedicated to spacer
48 acquisition, Cas1 and Cas2[22,23]. *Pseudomonas aeruginosa* has become a powerful
49 model organism for studying Type I CRISPR-Cas mechanisms[24-29], functions[3,23,30,31],
50 evolution[32-34], and interactions with phages utilizing anti-CRISPR proteins[35-38]. The *P.*
51 *aeruginosa* strain PA14 possesses an active Type I-F CRISPR-Cas immune system that
52 naturally targets many phages. The surveillance complex is composed of four Cas
53 proteins (Csy1, Csy2, Csy3, and Csy4), which are encoded together in a single
54 operon[26]. The surveillance complex is guided by CRISPR RNAs (crRNAs) originating
55 from one of two chromosomally encoded CRISPR arrays[26]. Finally, a separate operon is
56 responsible for the production of Cas1 and a Cas2-3 fusion protein, the latter of which
57 mediates nucleolytic destruction of target DNA.
58
59 To discover regulators controlling the transcription of the CRISPR-Cas surveillance
60 complex in *P. aeruginosa*, we utilized a *P. aeruginosa* strain PA14 engineered to
61 express *lacZ* in place of the *csy3* gene (*csy3::lacZ*)[39]. The *csy3*::*lacZ* reporter strain was
62 subjected to transposon mutagenesis and colonies isolated and screened on X-gal
63 plates. ~40,000 colonies were visually examined for increased or decreased levels of β-
64 galactosidase. Multiple independent insertions were identified that abolished LacZ levels
65 within *lacZ* and upstream genes (*csy1* and *csy2*), indicating successful mutagenesis and
66 screening. Thirty distinct mutants with transposon insertions outside of this region, with
67 altered β-galactosidase levels, were isolated and mapped. These mutants are listed in
68 Supplementary Table 1 with β-galactosidase levels quantified for mutants that grew well

69 in culture. Four independent insertions were identified in a single gene, *kinB*, which
70 resulted in apparent mucoidy plating morphology and decreased β-galactosidase
71 production (Supplementary Fig. 1a). Quantification of β-galactosidase levels in liquid
72 growth experiments revealed ~50% less *csy3::lacZ* expression compared to wild-type
73 (WT) PA14 for each mutant (Supplementary Table 1, Supplementary Fig. 1b). We next
74 focus on *kinB* (a sensor kinase/phosphatase) because it was the only gene with >1
75 independent transposon insertion and displayed the largest β-galactosidase activity
76 change.
77
78 To determine the consequences of *kinB* disruption and decreased *csy* expression on
79 CRISPR-Cas function, we measured the ability of *kinB::Tn* insertions to limit the
80 replication of phage. Phages used to assay activity are: DMS3$_{acrIE3}$ which is an
81 untargeted control phage, DMS3m$_{acrIE3}$ [40], which is fully targeted by the PA14 Type I-F
82 CRISPR-Cas system, and phage DMS3m $_{acrIF4}$, which is partially targeted, by virtue of
83 encoding a "weak" anti-CRISPR, *acrIF4,* that binds to the surveillance complex to inhibit
84 CRISPR-Cas function[35,37,41]. The *kinB::Tn* strains remained resistant to DMS3m$_{acrIE3}$
85 infection, but DMS3m$_{acrIF4}$ formed 10-fold more plaques relative to WT, demonstrating
86 attenuated CRISPR-Cas function (Figure 1a, Supplementary Fig. 1c). This defect was
87 complemented by expression of *kinB in trans* (Supplementary Fig. 1c). Growth of control
88 phage DMS3$_{acrIE3}$ was not impacted in the absence of KinB (Figure 1a). Furthermore,
89 two other targeted phages, JBD26 (naturally possessing *acrIF4*) and JBD25 (a partially
90 targeted phage with no Acr) also showed increased replication in the *kinB:Tn* strain
91 (Supplementary Fig. 1d) relative to WT PA14. Replication of a phage with a weak anti-
92 CRISPR or one that is targeted by a less active spacer is therefore a sensitive
93 barometer for perturbations in CRISPR-Cas levels. Together, these data confirm that in
94 the absence of *kinB, csy* gene expression and phage targeting are decreased.
95
96 KinB is a sensor kinase/phosphatase in a two-component system with response
97 regulator AlgB. The KinB/AlgB system has a large regulon within *P. aeruginosa*, but is
98 well-known for its role in biofilm regulation[42]. In the absence of KinB function, the activity
99 of the transcription factor AlgU (a σ^E orthologue and an activator of biofilm formation) is
100 enhanced[43,44]. This activation of AlgU manifests solely due to the lack of KinB
101 phosphatase activity and the resulting accumulation of the phosphorylated form of the
102 response regulator AlgB (P-AlgB). The phosphorylation of AlgB has been attributed to

103 unknown kinases[45,46] (Fig. 1b). The resulting accumulation of P-AlgB activates the
104 periplasmic protease AlgW (a DegS homolog), which degrades MucA, liberating sigma
105 factor AlgU[47,48,49] (Fig. 1b). AlgU positively regulates many factors involved in biofilm
106 production, including AlgR, AlgD, AlgB, and AmrZ[50-52].
107
108 To determine if this KinB-controlled biofilm activation pathway also regulates CRISPR-
109 Cas expression, we tested the ability of phosphatase and kinase dead KinB mutants to
110 complement an in-frame Δ*kinB* deletion, using the replication of the partially-targeted
111 DMS3m$_{acrIF4}$ phage as a metric for CRISPR-Cas activity. WT *kinB* or kinase inactive
112 H385A *kinB* (Fig. 1c) complemented the CRISPR defect, indicating KinB kinase activity
113 is dispensable for CRISPR-Cas activation. However, a P390S *kinB* mutant incapable of
114 dephosphorylating the response regulator AlgB did not complement, and in fact
115 decreased CRISPR-Cas activity further (Fig. 1c). This suggests that CRISPR-Cas
116 expression is inhibited by the accumulation of P-AlgB. A Δ*kinB*Δ*algB* double mutant
117 restored CRISPR-Cas targeting to WT levels (Supplementary Fig. 2a), confirming the
118 role of this signaling pathway. A strain lacking *algB* (Δ*algB*) or possessing a D59N
119 mutant that cannot be phosphorylated had elevated CRISPR-Cas activity, supporting the
120 repressive role of P-AlgB (Supplementary Fig. 2b). Together, these data suggest that
121 KinB-mediated dephosphorylation of AlgB lifts CRISPR-Cas inhibition, and conversely
122 accumulation of high levels of P-AlgB (achieved in Δ*kinB* or *kinB P390S*) leads to
123 CRISPR-Cas repression.
124
125 To assess CRISPR-Cas regulation downstream of P-AlgB, anti-phage immunity was
126 assayed in Δ*algU* and Δ*algR* backgrounds, revealing enhanced targeting of DMS3m$_{acrIF4}$
127 but not control phage DMS3$_{acrIE3}$ in each knockout (Fig. 1d). Complementation with *algR*
128 and *algU* restored CRISPR-Cas levels in their respective knockout backgrounds (Fig.
129 1d). This demonstrates that these proteins repress CRISPR-Cas immunity. Double
130 knockouts of each gene combined with Δ*kinB* each resembled the respective Δ*algU* and
131 Δ*algR* single knockouts, consistent with these factors acting downstream of KinB
132 (Supplementary Fig. 2a). The observed plaquing defects seen with the DMS3m$_{acrIF4}$
133 phage are CRISPR-dependent, as double knockouts (*kinB, algB, algU, algR* mutants
134 combined with *csy3::lacZ*) revealed plaquing equivalent to *csy3::lacZ* alone
135 (Supplementary Fig. 2c).
136

137 Phages that use anti-CRISPRs to inhibit CRISPR-Cas immunity must cooperatively
138 infect the same cell in order to produce a sufficient dose of anti-CRISPR to permit phage
139 replication[41,53]. The multiplicity of infection (MOI) required to overwhelm immunity is
140 dependent on the affinity of the anti-CRISPR for the CRISPR-Cas machinery and the
141 intracellular concentration of CRISPR-Cas complexes. To understand how this
142 regulatory pathway controls phage cooperation requirements on a population level by
143 potentially shifting the intracellular concentration of CRISPR-Cas complexes, liquid
144 cultures of Δ*algU* and Δ*kinB* mutants were infected with a virulent derivative of phage
145 DMS3m$_{acrIF4}$ at both high (where the WT cells are sensitive) and low (where the WT cells
146 are resistant) MOI (Figure 1e). The Δ*algU* mutant was able to limit phage replication
147 relative to WT and continue growing when infected with concentration of phages
148 sufficiently high to overwhelm WT immunity (10^6 PFU), indicating increased levels of
149 CRISPR-Cas machinery (Fig 1e). Conversely, when infected with a low MOI of phages
150 (10^4 PFU), all bacterial genotypes were able to grow to high cell density, however the
151 Δ*kinB* mutant permitted increased phage replication relative to WT, demonstrating a
152 decreased level of immune system components (Fig 1f). Importantly, these changes in
153 phage replication requirements were not seen in the absence of CRISPR-Cas immunity,
154 as phage replication in double knockouts *algU csy3::lacZ and kinB csy3::lacZ*
155 resembles *WT csy3::lacZ (*Supplementary Fig. 3a-d, f). In contrast, Δ*algR* demonstrated
156 CRISPR-independent phage resistance during liquid culture infection, and phage
157 cooperation requirements could not be reliably measured for this mutant (Supplementary
158 Fig. 3e). Taken together, these data demonstrate that a well-characterized biofilm
159 activation pathway controlled by alternate sigma factor, AlgU, represses CRISPR-Cas
160 immunity in *P. aeruginosa.*
161
162 As our screen was focused on finding regulators of the *csy* operon, and as Cas3 is
163 expressed at low levels and is furthermore subject to post-translational control by
164 Cas1[28], we hypothesized the KinB/AlgB pathway was controlling anti-phage immunity via
165 modulation of *csy* complex levels. To specifically measure the anti-phage activity of the
166 *csy* complex in the AlgU regulatory pathway mutants, we developed a Cas3-indepedent
167 bioassay to read out the activity of the surveillance complex in the cell. Through the
168 rational design of crRNAs to target an early phage phage promoter (P_E_1, P_E_2), we
169 observed inhibition of phage replication in a *P. aeruginosa* strain with a nuclease dead
170 Cas3 (Cas3$_{D124A}$, Figure 2a). This CRISPR-based transcriptional interference (CRISPRi)

171 effect was also seen when infecting with a phage that expressed the inhibitor of Cas3
172 recruitment, AcrIF3, but not an inhibitor that blocks Csy complex-phage DNA binding[37],
173 AcrIF1 (Figure 2a). CRISPRi was mediated by crRNAs targeting phage promoters,
174 including one (P_E_2) that completely limited phage replication in the absence of Cas3
175 activity, while an ORF-targeting crRNA was ineffective. We selected P_E_1 as a
176 moderately-functional CRISPRi spacer and expressed it in various mutant backgrounds
177 generated in this study. We observed decreased CRISPRi activity against phage
178 DMS3m$_{acrIF3}$ in the ΔkinB background, but increased CRISPRi-mediated phage
179 repression in Δ*algR* and Δ*algU,* (Figure 2b), demonstrating that modulation of *csy* gene
180 expression by this pathway impacts phage targeting in a Cas3-independent manner. To
181 confirm that this pathway controls the levels of *csy* complex in the cell, we fused an N-
182 terminal sfCherry tag to the endogenous *csy1* gene in the mutant backgrounds. We
183 observed decreased levels of red fluorescence in Δ*kinB* and increased levels in Δ*algR*
184 and Δ*algU* relative to WT, demonstrating that this pathway controls the levels of *csy*
185 complex in the bacterial cell (Fig. 2c).
186
187 AlgU and AlgR are proteins that regulate hundreds of genes in *P. aeruginosa*[54-56],
188 ultimately repressing acute virulence factors (e.g. pyocyanin) and activating chronic
189 virulence factors (e.g. biofilm production). To identify downstream CRISPR-Cas
190 regulators, we considered the large AlgU regulon[56], but focused on a factor involved in
191 biofilm production, whose expression is AlgU-dependent, *amrZ*[51,57]. AmrZ is a ribbon-
192 helix-helix type transcription factor, and acts as both a repressor and activator of
193 transcription in *Pseudomonas*[58]. We generated a knockout of *amrZ* and observed a
194 CRISPR-dependent (Supplementary Fig. 2c) decrease in DMS3m$_{acrIF4}$ plaque formation
195 (Fig. 3a). This was complemented when *amrZ* was expressed *in trans* (Fig. 3a),
196 indicating that AmrZ is also a repressor of CRISPR-Cas immunity. However, when we
197 measured phage cooperation requirements in the Δ*amrZ* strain, phage replication and
198 immune protection did not differ substantially from from WT (Fig. 3b,c). The most
199 obvious difference between the phage plaque assay and the assay to measure phage
200 cooperation is that a plaque assay is performed on solid plates whereas phage
201 cooperation requirements were measured in liquid culture. To test if AmrZ was a
202 surface-specific repressor of CRIPSR-Cas immunity, we measured the levels of Csy
203 complex during surface association and planktonic growth in WT and Δ*amrZ* cells using
204 the endogenous Csy1-sfCherry reporter. In WT cells, the levels of Csy complex were

205 attenuated during surface-association relative to planktonic growth, but in the absence of
206 AmrZ, Csy complex levels during surface association increased to levels comparable to
207 those in planktonic growth (Fig. 3d). Deletion of *amrZ* did not impact Csy complex levels
208 during planktonic growth (Fig. 3e). To artificially increase the levels of AmrZ during
209 planktonic growth, we ectopically expressed AmrZ from a high copy plasmid. In this
210 scenario, high levels of AmrZ were sufficient to repress Csy complex expression,
211 suggesting that low AmrZ activity in planktonic growth underlies its surface-specific
212 control of CRISPR-Cas (Fig. 3f). In contrast to AmrZ, the transcriptional repressors AlgU
213 and AlgR were unable to repress Csy complex levels when heterologously expressed
214 (Fig. 3f), likely because they are master regulators and many redundant mechanisms
215 are in place to control their activity. Taken together, these data demonstrate that AmrZ is
216 a uniquely potent surface-specific repressor of the *csy* operon.

217 We next considered if phages and other mobile genetic parasites naturally antagonized
218 by CRISPR-Cas immunity had evolved mechanisms to manipulate this repressive
219 pathway. Inspired by a recent discovery of a *Paraburkholderia* phage that carried a
220 distant homolog of AmrZ[59], we searched the NCBI database for AmrZ homologs on
221 *Pseudomonas* mobile genetic elements (MGE). Surprisngly, we identified 14 diverse
222 *Pseudomonas* genetic parasites carrying AmrZ homologs (Supplementary Table 2).
223 These MGEs included obligately lytic and temperate Myoviridae, temperate
224 Siphoviridae, and plasmids. AmrZ has been structurally characterized in complex with
225 operator DNA[58], and these mobile AmrZ homologs showed perfect conservation of
226 critical DNA-interacting residues in the ribbon-helix-helix domain, suggesting conserved
227 binding specificity (Fig. 4a, b, red residues/arrowheads). To test if these mobilized AmrZ
228 variants were capable of regulating CRISPR-Cas activity in *Pseudomonas aeruginosa*,
229 we synthesized 2 phage-borne *amrZ* homologs and tested them for their ability to
230 complement the Δ*amrZ* strain. Both homologs complemented the Δ*amrZ* mutant,
231 indicating they were active in the PA14 transcriptional network and were *bona fide* AmrZ
232 orthologs (Fig. 4c). Next, each phage gene was expressed in WT cells, revealing one
233 homolog ($amrZ_{phi3}$) limited the expression a Csy1-sfCherry reporter. This suggests the
234 possibility that *amrZ* has been hijacked for its capacity to inhibit CRISPR-Cas expression
235 (Fig. 4d). Thus, *amrZ* acts on both sides of the battle between bacteria and mobile
236 genetic elements.
237

238 **Discussion**

239 The factors that govern expression of bacterial processes are highly variable across
240 species, reflecting niche-specific adaptations. CRISPR-Cas immune systems limit the
241 replication of foreign genetic elements, but few reports address how the regulation of
242 CRISPR-Cas impacts phage targeting. Here, we utilized a genetic screen that identified
243 KinB as a positive regulator of CRISPR-Cas function in *P. aeruginosa.* This sensor
244 kinase/phosphatase operates in a two-component system with AlgB that regulates a
245 well-characterized biofilm-stimulatory pathway, though the ligand for KinB remains
246 unknown. Removal of KinB or inactivation of its phosphatase activity leads to the
247 accumulation of P-AlgB, which stimulates the activity of CRISPR-Cas repressors AlgU,
248 AlgR, and AmrZ. This pathway is well-studied due to the recurrent isolation of alginate-
249 overproducing (mucoid) *P. aeruginosa* from the lungs of cystic fibrosis patients, with
250 mutations in *mucA*[60] and *kinB*[47,61] that lead to the constitutive activation of AlgU. This
251 biofilm pathway generates the characteristic mucoidy phenotype of CF *P. aeruginosa*
252 isolates[43,62,63], which we also observed in *kinB:Tn* mutants (Supplementary Fig. 1a).

253 This pathway is well described in its capacity to activate biofilm production, and here we
254 show that this transcriptional network also functions to dampen CRISPR-Cas activity in
255 non-biofilm conditions. In WT cells, KinB phosphatase activity increases CRISPR-Cas
256 function, though the effect is relatively mild in our experimental conditions. Relieving
257 transcriptional repression via deletion of *algU* or *algR* however leads to a hyper-
258 activation of the CRISPR-Cas immune response. We further demonstrate that *amrZ* acts
259 in this pathway to specifically repress CRISPR-Cas when cells are surface-associated,
260 leading to lower levels of *csy* complex during surface-association relative to planktonic
261 growth. Phages and plasmids have taken advantage of this regulatory scheme, and
262 some *Pseudomonas* genetic parasites carry hijacked copies of the CRISPR-Cas
263 repressor *amrZ*. We show that these mobilized *amrZ* homologs retain their capacity to
264 transcriptionally repress CRISPR-Cas, demonstrating a dual role for this gene in the
265 host-pathogen arms race between bacteria and their parasites.
266
267 Considering the physiology of *P. aeruginosa* can put these findings into context with a
268 phage and CRISPR-Cas-centric view. During exponential growth is when we and others
269 observe CRISPR-Cas activation[8,9], and is also when phage infection risk is likely high
270 (i.e. metabolically active, well-mixed planktonic cultures at high cell density[33]).

271 Conversely, surface-association lessens phage infection risk, as spatial structure limits
272 phage diffusion and prevents a phage bloom from overtaking the entire bacterial
273 population[64]. Though we do not measure phage sensitivity in a biofilm here, biofilm
274 production likely provides an even greater level of intrinsic phage resistance, due to high
275 levels of spatial stratification and abundant polysaccharide secretion.

276 Supporting our proposal that *P. aeruginosa* surface-association/biofilm formation and
277 CRISPR-Cas expression are inversely correlated are two independent observations: **i)**
278 our analysis of a previously published PA14 RNAseq data set[65] and proteomic data set[66]
279 revealed activation of CRISPR-Cas expression in exponential phase, and strong
280 transcriptional repression during stationary phase and biofilm growth (Supplementary
281 Fig. 4a). Interestingly Cas proteins are still detected in stationary phase and biofilm
282 growth, suggesting the cells retain some immune-competency even after transcriptional
283 shutdown (Supplementary Fig. 4b), and **ii)** previous studies on the *P. aeruginosa*
284 CRISPR-Cas system have revealed that the genome is hyper-sensitive to CRISPR-
285 induced DNA damage during surface-association and biofilm formation, leading to cell
286 death when a mismatched prophage sequence target is present in the chromosome[30,31].
287 This suggests that CRISPR auto-immunity costs are also dependent on the growth state
288 and physical environment of the cell, and that CRISPR-Cas regulation in *P. aeruginosa*
289 is tuned to reflect this intrinsic sensitivity.

290 Here, we report the identification of a CRISPR-Cas repressive pathway in *P. aeruginosa*.
291 Phages bearing distinct anti-CRISPRs are employed in bioassays to read out the activity
292 of the CRISPR-Cas surveillance complex. Using a CRISPRi phage-repression assay,
293 coupled with translational reporters, we conclude that *algU*, *algR*, and *amrZ* control the
294 production of the CRISPR surveillance complex (*csy* complex), which is where the
295 screen was focused. Interestingly, our observations show that CRISPR-Cas activity in *P.*
296 *aeruginosa* does not operate at full strength, despite the capacity of a hyper-activated
297 immune system to severely limit the replication of phages relying on anti-CRISPRs for
298 survival. We speculate that the ability to control CRISPR-Cas activity during lifestyle
299 transitions may be essential for *P. aeruginosa* to safely maintain a CRISPR-Cas system
300 by limiting self-toxicity. Furthermore, we reveal an unexpected cost to negative
301 regulation of CRISPR-Cas immunity in our discovery of MGE-encoded CRISPR-Cas
302 repressors: though CRISPR-Cas control is likely essential for safe retention of the
303 immune system, the evolution of potent mechanisms of CRISPR-Cas repression has

304 created an Achilles Heel that is exploited by genetic parasites.

305 **Acknowledgements**
306 The Bondy-Denomy lab was supported by the University of California, San Francisco
307 Program for Breakthrough in Biomedical Research, funded in part by the Sandler
308 Foundation, and an NIH Office of the Director Early Independence Award (DP5-
309 OD021344), and R01GM127489. We thank Deborah Hung's lab for providing Δ*kinB,*
310 Δ*algR,* Δ*algU* strains and associated mutants. George O'Toole's lab provided the
311 *csy3::lacZ* PA14 strain.
312

313 **Author Contributions**
314 J.B.D., A.L.B, and B.C. formulated study design and plans. A.L.B. designed and
315 conducted bacteriophage plaque assays, liquid infection assays, and CRISPRi assays,
316 performed. B.C. conducted the genetic screen, isolated and constructed bacterial
317 mutants, conducted LacZ expression profiling, and performed bacteriophage plaque
318 assays. CRISPR-Cas expression profiling, and conducted bioinformatics analyses. S.G.
319 designed, constructed, and validated sfCherry reporter strains. T.S. conducted CRISPRi
320 assays and V.E. assisted in establishing fluorescent reporter assays. J.B.D. and A.L.B
321 wrote the manuscript.
322

323 **Competing Interests**
324 J.B.-D. is a scientific advisory board member of SNIPR Biome and Excision
325 Biotherapeutics and a scientific advisory board member and co-founder of Acrigen
326 Biosciences.
327

328 **Materials & Correspondence**
329 Correspondence should be directed to joseph.bondy-denomy@ucsf.edu
330

331 **Methods**
332 **Bacterial strains and bacteriophages.** *P. aeruginosa* UCBPP-PA14 (PA14) strains
333 and *E. Coli* strains (Sup. Table) were grown on lysogeny broth (LB) agar or liquid at 37
334 ^{o}C. Media was supplemented with gentamicin (50 µg ml^{-1} for *P. aeruginosa* and 30 µg ml^{-}
335 ^{1} for *E. Coli*) to maintain the pHERD30T plasmid or carbenicillin (250 µg ml^{-1}) for *P.*
336 *aeruginosa* or ampicillin (100 µg ml^{-1}) for *E. coli* containing the pHERD20T plasmids.

337 pHERD plasmids were induced with 0.1% arabinose. Bacteriophages stocks were
338 prepared as described previously[40]. In brief, 3 ml of SM buffer was added to plate
339 lysates of the desired purified bacteriophage and incubated at room temperature for 15
340 minutes. SM buffer containing phages was collected and 100 µl of chloroform was
341 added. This was centrifuged at 10,000 x g for 5 minutes and supernatant containing
342 phages was transferred to a screw cap storage tube and incubated at 4 ^{o}C.
343
344 **Tn mutagenesis screen.** The *csy*::*lacZ* reporter strain was subjected to transposon
345 mutagenesis and colonies were isolated on plates containing X-gal (5-bromo-4-chloro-3-
346 indolyl-β-D-galactopyranoside). ~50,000 colonies were visually examined for increased
347 or decreased levels of β-galactosidase and insertions mapped by semi-random PCR. To
348 conduct transposon mutagenesis, overnights of PA14 *csy3::lacZ* and *E. coli* containing
349 the pBTK30 Tn suicide vector were mixed in a 1:2 ratio (donor : recipient) for
350 conjugation. A second control group containing PA14wt and *E. Coli* containing the
351 pBTK30 Tn suicide vector was set up in parallel. Mixed cells were centrifuged at 4,000 x
352 g for 10 minutes to pellet cells. 100 µl of resuspended conjugation pellet was then
353 spotted on LB agar plates and incubated at 37 ^{o}C for 6hrs. Conjugation spots were
354 collected and resuspended in LB liquid media. Conjugation was then screened on an LB
355 agar plates supplemented with nalidixic acid (30 µg ml^{-}1) and gentamicin (50 µg ml^{-1}).
356 Surviving colonies containing Tn insertions were collected into 1ml of LB liquid media.
357 Serial dilution of were prepared and plated on LB agar plates supplemented with x-gal
358 (200 µg ml^{-1}) and gentamicin (50 µg ml^{-1}) and nalidixic acid (30 µg ml^{-}1). Plates were
359 incubated at 37 ^{o}C for 24 hours to allow for colonies to change color. Colonies displaying
360 changed expression levels as compared to our positive control (PA14 csy3::lacZ no
361 pBTK30) were then isolated onto secondary LB agar plates with X-gal and gentamicin
362 and nalidixic acid at the stated concentrations. Genomic DNA (gDNA) was collected
363 from isolated single colonies by resuspending bacterial colonies in 0.02% SDS and
364 boiling the sample for 15 minutes. Samples were then centrifuged at 10,000 x g and
365 supernatants containing gDNA were collected. Semi-random PCR was then performed
366 using PCR primers listed on sup table_. PCR samples were sequenced and reads were
367 then matched to the *P. aeruginosa* UCBPP-PA14 genome using BLAST. Isolated
368 containing genes of interest were saved as stocks (s. table 1). Transcription changes
369 were then verified via modified β-galactosidase assay.
370

371 **Plaque assays.** Plaque assays were performed on LB agar plates (1.5% agar) with LB
372 top agar (0.7% agar), both supplemented $MgSO_4$ (10 mM final concentration) and
373 gentamicin (50 µg ml^{-1}) as needed for plasmid maintenance. Spot titrations were done by
374 mixing 150 µl of a *P. aeruginosa* overnight culture with 3 ml of top agar, which was
375 dispersed evenly on a LB $MgSO_4$ plate. 3 µl of 10-fold phage dilutions were then spotted
376 on the surface. Plates were incubated overnight at 30 ^{o}C. To count plaques, full plate
377 assays were used, except when CRISPR-targeting was so strong that discrete plaques
378 could not be accurately measured. In this case, spot titrations are shown. For full plate
379 assays, 3 µl of the selected phage dilution was incubated with 150 µl of *P. aeruginosa*
380 overnight for 15 minutes at 37 ^{o}C. 3 ml of top agar was then added and the mixture was
381 dispersed evenly on a LB $MgSO_4$ plate. Individual plaques were then counted to assess
382 differences in plaquing efficiency.
383
384 **β-galactosidase assay.** A modified version of the previously described β-galactosidase
385 assay was used to measure *lacZ* activity in transcriptional fusions. Bacterial cultures
386 were grown overnight at 37 ^{o}C. Cultures were then diluted 1:100 into LB liquid medium
387 supplemented with the desired antibiotic. Diluted cultures were then incubated at 37 ^{o}C
388 until the desired time point was reached. Culture density was measured with a
389 spectrophotometer (OD_{600}) and 200 µl of the sample was added 800 µl to
390 permeabilization solution (components listed in sup table XX). Cells were mixed via
391 inversion and vortexed for 1 minute to permeabilize the cells. 200 µl of ONPG (4 mg ml^{-}
392 ^{1}) was added and samples were incubated for 27 minutes at 30 ^{o}C. Enzymatic reaction
393 was stopped by addition of 300 µl of 1M Na_2CO_3. Samples were centrifuged at 13,000 x
394 g for 5 minutes to remove debris and 200 µl of supernatant was moved to a 96-well plate
395 to read absorbance at 420 nm and at 550 nm. Miller units were calculated using the
396 Miller equation. 3 technical replicates per sample per experiment.
397
398 **Phage transduction of *kinB::Tn* alleles.** Transposon insertions in *kinB* from a
399 *csy3::lacZ* background were transduced into WT PA14 to enable testing of CRISPR-Cas
400 function with the same transposon insertion. Phage phiPA3 was used to infect the donor
401 strain (*csy3::lacZ, kinB::Tn*), on plates with top agar overlays, using ~10^4 PFU to
402 generate near confluent lysis. Plates were soaked in 3-4 mL of phage SM buffer and 2
403 mL collected over chloroform, vortexed, and pelleted to isolate transducing phage in the
404 supernatant. Lysates were used to infect recipient strains (WT PA14). ~10^8 PFU were

405 used to infect a culture at an MOI of 1. After 30 minutes of static incubation on the
406 bench, cultures were gently shaken at 37 ^{o}C for 20 min and then pelleted at 5000 x g.
407 Cells were washed twice with LB, and subsequently incubated at 37 ^{o}C for 1 hour to
408 allow recombination and gentamicin resistance outgrowth. Cultures were pelleted and
409 resuspended in 200 µL of LB, and plated on LB plates containing gentamicin. Controls
410 included uninfected cells and cells infected with phages not propagated on a gentamicin
411 resistant donor strain. Additionally, phage lysate was directly plated under selection to
412 confirm no residual donor strain in the phage preparation. Plates were incubated
413 overnight at 37 ^{o}C and their identity (i.e. CRISPR-Cas intact) confirmed with a plaque
414 assay using DMS3m as the target phage and PCR of the kinB locus.
415
416 **Introduction of *csy3::lacZ P. aeruginosa* UCBPP-PA14 strains.** The *lacZ* gene was
417 introduced into PA14 strains of interest via homologous recombination. Recombination
418 vector containing lacZ flanked by homology arms matching csy2 and csy4 was
419 introduced via conjugation. PA14 strains and *E. coli* containing vector were mixed at a
420 ratio of 1:2 (recipient:donor). Mixture was heat shocked at 42 ^{o}C for 10 min. Mating spot
421 was then plated on a LB agar plate and incubated overnight for 30 ^{o}C. Mating spot was
422 then collected, resuspended in 1 ml of LB liquid media and plated on VBMM plates
423 supplemented with 50 ug/mL gentamicin to select for colonies with the integrated
424 homology plasmid. Colonies were cultured overnight in LB in the absence of selection at
425 37 ^{o}C, and were then diluted and counterselected on no salt LB (NSLB) agar plates
426 supplemented with 15% sucrose. Surviving colonies were then grown on LB agar plates
427 supplemented with gentamicin and X-gal to check for *lacZ* insertion via color change and
428 lacZ insertion was further verified via PCR.
429
430 **Generation of an PA14*ΔamrZ* strain using the endogenous I-F CRISPR-Cas**
431 **system.** Complementary oligonucleotides encoding a crRNA targeting the *amrZ* gene of
432 PA14 were annealed and ligated into the multiple cloning site of the pHERD30T vector.
433 A fragment possessing homology arms flanking the desired mutation (500 bp upstream
434 and 500 bp downstream) around *amrZ* was cloned into a distinct location (NheI site) of
435 the same vector via Gibson assembly. The new plasmid containing both a crRNA and
436 homology region was introduced into WT PA14 via electroporation. Transformation
437 efficiency dropped dramatically in the presence of the crRNA due to the toxicity caused
438 by self-targeting. All surviving colonies had the desired clean deletion of the *amrZ* gene.

439 Deletions were confirmed by PCR of the region of interest and subsequent Sanger
440 sequencing of the amplicon. A 2000 bp region flanking *amrZ* was PCR amplified and
441 sequencing primers were designed to sequence both the deletion junction and outside of
442 the original 500 bp flanking regions to confirm the removal of the *amrZ* gene.
443
444 **Liquid phage cooperation assay**. Liquid phage infections were performed as
445 described in[41]. In brief, an overnight culture of cells was diluted 1:100 into fresh media,
446 and infected with virulent phage DMS3m$_{acrIF4}$ in biological triplicate in a 96 well Costar
447 plate. Cells were incubated at 37 ^{o}C with constant rotation and OD600 measured every 5
448 minutes in a Biotek H4 Synergy plate reader. Phage were harvested from each well and
449 quantified by plaque assay after 24 hours.
450
451 **Generation of endogenous Csy1-sfCherry reporter.** Endogenous Csy1-sfCherry
452 reporter was constructed similar to the construction of *csy3::lacZ.* We initially verified
453 that tagging of sfCherry at the N-terminus of *csy1* is functional, when expressed from a
454 plasmid. pMQ30-sfCherry-Csy1, which contains sfCherry sequence flanked by 657 bp
455 upstream of csy1 and 701 bp downstream of csy1 start codon, was cloned in pMQ30
456 plasmid between HindIII and BamHI sites using Gibson assembly. The Csy1-sfCherry
457 construct was introduced into PA14 strains of interest via homologous recombination.
458 Strains containing Csy1-sfCherry insertion were verified via PCR.
459
460 **Csy1-sfCherry reporter profiling**. **Liquid**: Cells were diluted 1:100 from an overnight
461 culture into fresh LB (with antibiotics and inducer if required), and grown for the indicated
462 number of hours in biological triplicate. 500 µl of each sample was then spun down at
463 8,000xg for 2 minutes, and resuspended in 500 µl of M9 media. Samples were loaded in
464 to a 96 well plate (150 µl /well) in technical triplicate and red fluorescence and OD600
465 were measured using a Biotek H4 Synergy. **Solid:** Cells were diluted 1:100 from an
466 overnight culture into fresh LB and 20 µl plated onto individual wells in biological
467 triplicate in a 24 well plate with each well containing solidified 1.5% LB Agar with
468 antibiotics and inducer if required. The 24 well plate was then covered with a breathable
469 Aeraseal, and incubated at 37 ^{o}C with no shaking. At the indicated timepoint, cells were
470 harvested by flooding each well with 500 µl of M9 buffer, and were spun down at
471 8,000xg for 2 minutes, and resuspended in 500 µl of M9 media. Sample were loaded in
472 to a 96 well plate (150 µl /well) in technical triplicate and red fluorescence (excitation

473 580 nm, emission 610 nm) and OD600 were measured using a Biotek H4 Synergy. To
474 calculate the relative fluorescence units for each sample, the background fluorescence
475 and background OD600 values obtained were subtracted from the sample values, and
476 the sample fluorescence was then normalized to the sample OD600.
477
478 **AmrZ homolog discovery and characterization.** BLASTp was used to search the
479 nonredundant protein database for AmrZ homologs (accession: ABJ12639.1) in
480 *Pseudmonas sp.* (taxid: 286) in May 2019. This homolog list (e value > 0.001) was then
481 examined for homologs found on phage or plasmid genomes. Representative homologs
482 were aligned using Clustal and the alignment visualized in Jalview, and key conserved
483 residues were mapped onto the structure in Pymol (PDB ID: 3QOQ). Select homologs
484 were synthesized (TWIST Biosciences) and cloned into the SacI/PstI site of the
485 arabinose-inducible plasmid pHERD30T using Gibson assembly. Vectors were
486 electroporated into *Pseudomonas aeruginosa* strains for functional testing, where they
487 were induced with 0.1% arabinose and maintained with 50 ug/mL gentimicin.
488
489
490

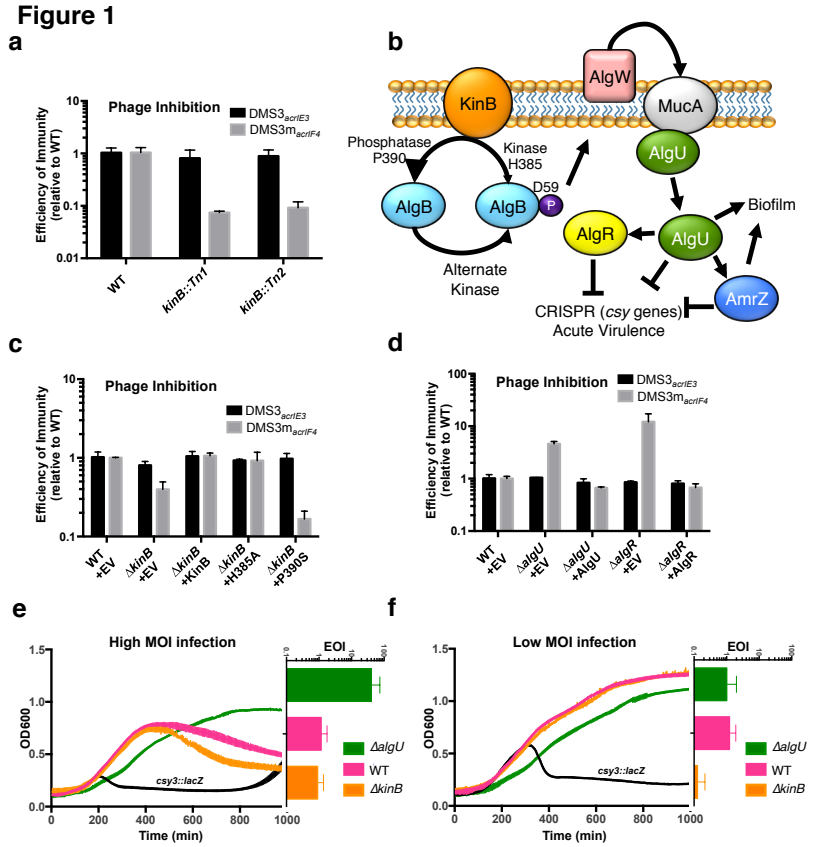

Figure 1: ***A forward genetic screen identifies a role for a biofilm activating pathway in repressing CRISPR-Cas immunity.*** **a**. Efficiency of immunity (EOI) against isogenic phages DMS3$_{acrIE3}$ (non-targeted) and DMS3m$_{acrIF4}$ (CRISPR-targeted). Plaque forming units (PFUs) were quantified on two independent *kinB* transposon mutants (*kinB::Tn1* and *kinB::Tn2*), then represented as a ratio relative to the number of PFUs measured on WT PA14. **b.** A cartoon summarizing the KinB/AlgB two component system and downstream effects, based on prior work, with CRISPR-Cas regulation added. **c**,**d** EOI measurements for indicated Δ*kinB,* Δ*algR,* and Δ*algU* strains with complementation. **e,f**. Growth curves of PA14 WT, Δ*algU*, or Δ*kinB* strains infected with either a high (e,10^6 PFU) or low (f, 10^4 PFU) MOI of virulent DMS3m$_{acrIF4}$. Phage replication was quantified as PFUs after 24 hours, and the efficiency of immunity expressed as a ratio of the number of PFUs harvested from the mutant strain compared to the number of PFUs obtained from WT. All data (OD600 and EOI measurements) are

505 represented as the mean of 3 biological replicates +/- SD.

Figure 2

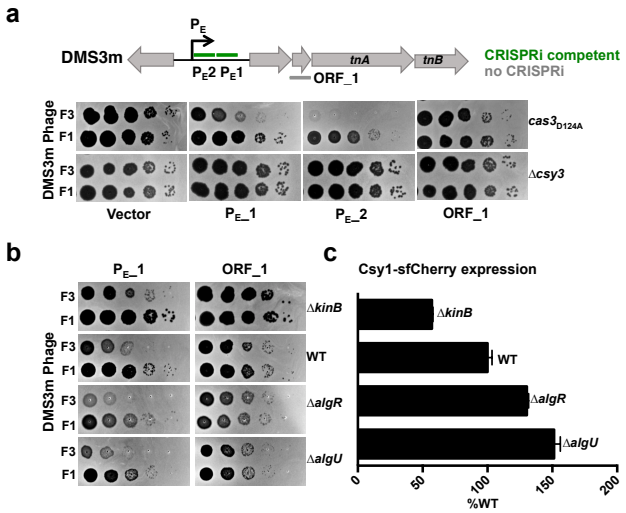

506

507

508 **Figure 2.** ***The kinB/algB pathway modulates Csy complex levels and activity.***

509 **a**. Spot titration of DMS3m$_{acrIF3}$ (F3) and DMS3m$_{acrIF1}$ (F1) on *cas3*$_{D124A}$ (dead Cas3) or
510 ∆csy3 (active Cas3, no Csy complex). Phages are targeted by natural spacer CR2_1, as
511 well as crRNAs designed to target DMS3m genome in positions designated on ORF
512 map. **b**. Spot titration of DMS3m$_{acrIF3}$ and DMS3m$_{acrIF1}$ phages on deletion mutants
513 expressing the indicated crRNA. **c.** Measurement of the normalized fluorescence levels
514 of Csy1-sfCherry reporter strains after 10 hours of growth in liquid culture. Fluorescence
515 measurements are represented as the mean of 3 biological replicates +/- SD.

516

517

Figure 3

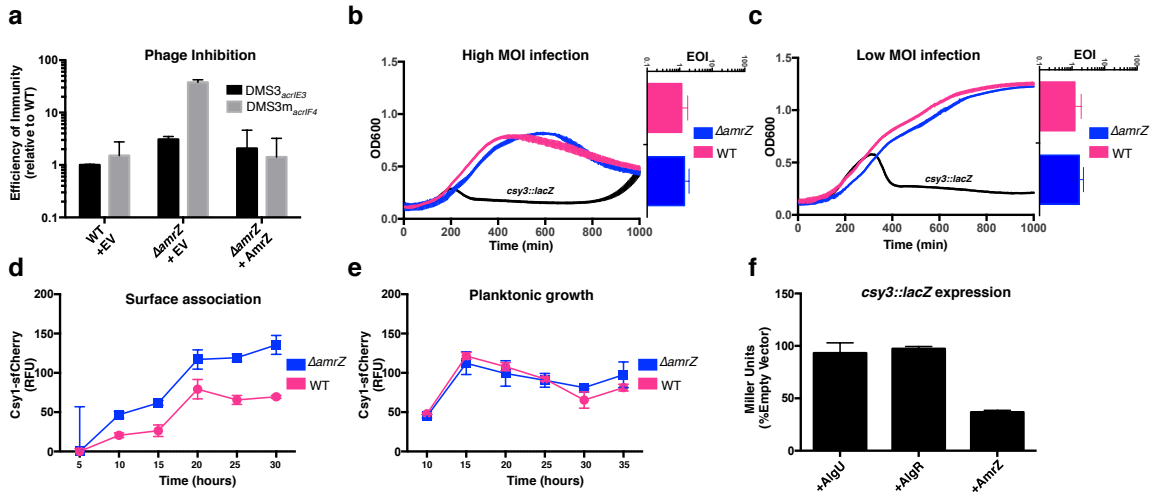

518

519 **Figure 3:** ***AmrZ is a surface-specific repressor of CRISPR-Cas immunity.*** **a**.
520 Efficiency of immunity (EOI) against isogenic phages DMS3$_{acrIE3}$ (non-targeted) and
521 DMS3m$_{acrIF4}$ (CRISPR-targeted). Plaque forming units (PFUs) were quantified on ΔamrZ
522 or the complemented strain, then represented as a ratio of the number of PFUs
523 measured on WT PA14. EOI measurements are represented as the mean of 2 biological
524 replicates +/- SD. **b,c**. Growth curves of PA14 WT and Δ*amrZ* infected with either a high
525 (d,10^6 PFU) or low (e, 10^4 PFU) MOI of virulent DMS3m$_{acrIF4}$. Phage replication was
526 quantified as PFUs after 24 hours, and the efficiency of immunity expressed as a ratio of
527 the number of PFUs harvested from Δ*amrZ* to the number of PFUs obtained from WT.
528 OD600 and EOI measurements are represented as the mean of 3 biological replicates
529 +/- SD. **d, e**. Timecourse of the relative fluorescence levels of Csy1-sfCherry reporter
530 strains during surface-association (d) or planktonic growth (e). Fluorescence
531 measurements are represented as the mean of 3 biological replicates +/- SD. **f**.
532 Overexpression of the indicated gene in a WT *csy3::lacZ* background, with Miller units
533 measured at 8h and normalized to empty vector.

Figure 4

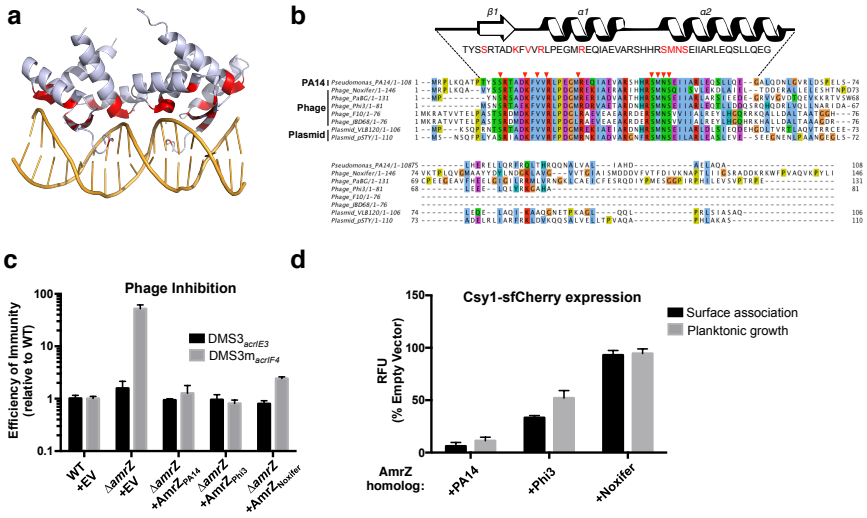

Figure 4. **Phage AmrZ homologs control CRISPR-Cas immunity. a.** Structure of an AmrZ tetramer bound to 18bp of operator DNA[58] with DNA-contacting residues highlighted in red. **b.** Protein alignment of seven mobile AmrZ homologs and the native PA14 AmrZ homolog, with the ribbon-helix-helix DNA binding domain secondary structure schematized and DNA-contacting residues indicated with red arrows and text. **c.** Efficiency of immunity (EOI) against isogenic phages DMS3$_{acrIE3}$ (non-targeted) and DMS3m$_{acrIF4}$ (CRISPR-targeted). Plaque forming units (PFUs) were quantified on ΔamrZ or the strains complemented with bacterial or phage AmrZ homologs, and represented as a ratio under the number of PFUs measured on WT PA14. EOI measurements as represented as the mean of 3 biological replicates +/- SD. **d.** Measurement of the normalized fluorescence levels of Csy1-sfCherry reporter strains transformed with bacterial or phage AmrZ homologs after 10 hours of growth in liquid culture or 20 hours of growth on solid media. Fluorescence measurements are represented as the mean of 3 biological replicates +/- SD.

Supplementary Table 1

Gene with Tn insertion	Transposon location	β-gal activity (% of unmutagenized)
kinB (1)	6448519	59%
kinB (2)	6447945	50%
kinB (3)	6447811	53%
kinB (4)	6449373	54%
kinB (5)	6449345	98%
purM	4618060	134%
lasR	4085810	135%
minD	1915545	N/D (growth defect)
gltB	5943637	108%
S-type pyocin	1196879	145%
pyoS3A	4404303	145%
tolA	4595505	158%
glycosyl transferase	5889967	81%
bacA	3490006	75%
Intergenic; zipA and smc +	3979746	N/D (growth defect)
gidB	6530337	88%
deaD	2373899	N/D (growth defect)
polA	6457284	N/D (growth defect)
pchH	798159	131%
crc	6275250	91%
putative plasmid stabilization protein	5347104	N/D (growth defect)
paraquat inducible protein	5532785	108%
pchH	797705	127%
yhiH/yhiI	6162134	108%
oxidoreductase FMN binding	4188602	N/D (growth defect)
putative membrane protein	1400718	118%
Intergenic; fstA and fstZ	5104077	111% (growth defect)
putative Zn-dependent oxidoreductase	2820446	115% (growth defect)
gnyL	3434168	87%
cytochrome c1 precursor	5126449	94%

549

550 **Supplementary Table 1**

551 All independent transposon insertions identified and mapped by visual screening with
552 increased or decreased *csy3::lacZ* β-galactosidase activity at 8 hours of growth. The
553 insertion location in the PA14 genome is shown, along with the measured level of β-
554 galactosidase enzyme. These measurements were not determined (N/D) for strains with
555 a growth defect.

Supplementary Table 2

Name	Accession	MGE type
PA14 AmrZ	ABJ12639.1	
Pseudomonas phage Noxifer	ARV77275.1	Lytic Myovirus
Pseudomonas phage phi3	YP_009276432.1	Integrated prophage
Pseudomonas phage PaBG	YP_008433620.1	Lytic Myovirus
Pseudomonas phage SM1	ALT58107.1	Siphoviridae (temperate)
Pseudomonas phage F10	YP_001293379.1	Siphoviridae (temperate)
Pseudomonas phage JBD68	ARM70500.1	Siphoviridae (temperate)
Pseudomonas sp. VLB120 plasmid pSTY	AGZ38169.1	Plasmid
Pseudomonas putida plasmid pKF715B	BAW27310.1	Plasmid
Pseudomonas veronii plasmid PVE_plasmid	SBW85251.1	Plasmid
Pseudomonas koreensis plasmid p3	AVX93364.1	Plasmid
Pseudomonas sp. Leaf58 plasmid pBASL58	AYG48213.1	Plasmid
Pseudomonas sp. XWY-1 plasmid	AUZ62175.1	Plasmid
Pseudomonas putida KF715C_pA870	BAW26592.1	Plasmid
Pseudomonas putida S12 plasmid pTTS12	AJA17154.1	Plasmid
Pseudomonas putida p12969-DIM	ALZ46341.1	Plasmid

Supplementary Table 2:

AmrZ homologs listed by the genome that encodes them, the accession number, and the mobile genetic element type.

Supplementary Figure 1

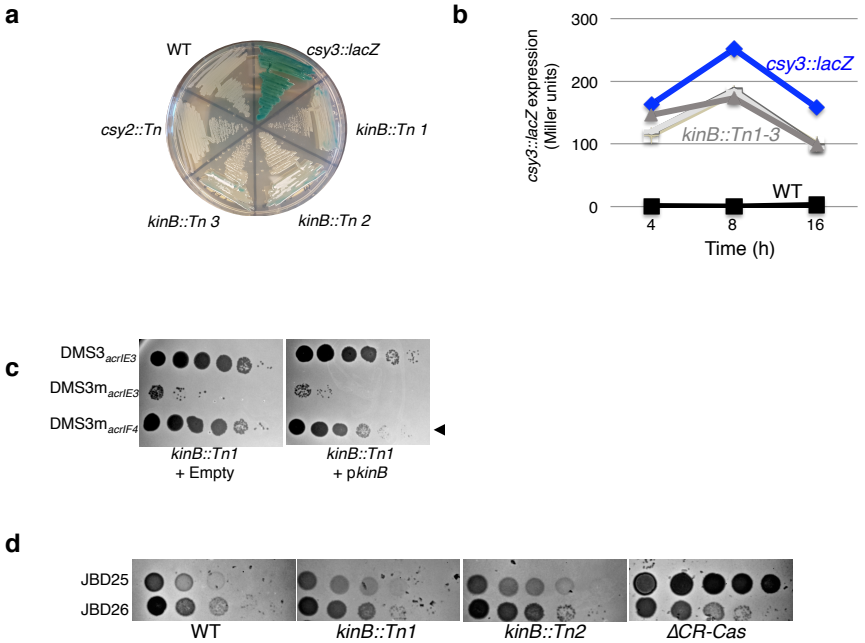

Supplementary Figure 1

a. A streak plate on X-gal plates, showing strains involved in this study and isolated transposon (Tn) insertions. **b**. β-galactosidase measurements at the indicated time points for the unmutagenized (*csy3::lacZ*) strain and three isolated *kinB* transposon mutants (*kinB::Tn1-3*). **c**. Phage titration on lawns of the *kinB::Tn1* mutant transformed with empty vector or *kinB.* **d.** Spot titration of phages JBD26 (CR2_sp17, sp20-targeted, possessing *acrIF4*), JBD25 (CR1_sp1 targeted) on *kinB::Tn* mutants and ΔCRISPR-Cas.

Supplementary Figure 2

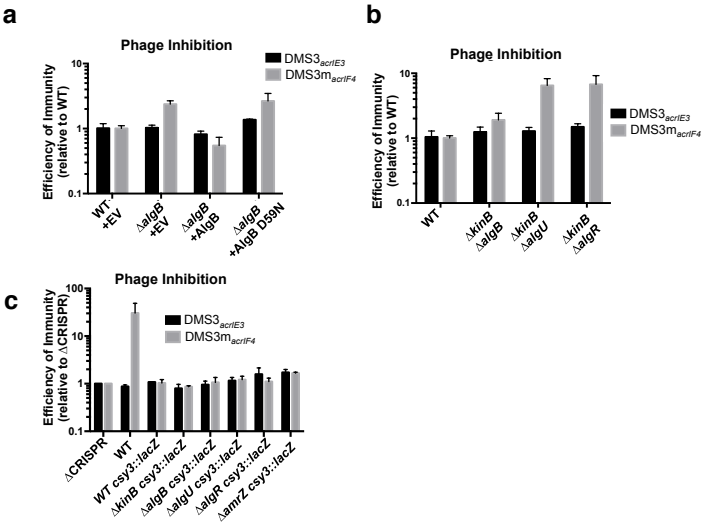

Supplementary Figure 2:

a-c. Efficiency of immunity measurements for indicated mutants relative to WT. **a**. Δ*algB* mutant complemented. **b.** Double knockouts show Δ*kinB* combined with *algB*, *algU*, or *algR*. **c**. Indicated knockouts were combined with *csy3::lacZ*.

Supplementary Figure 3

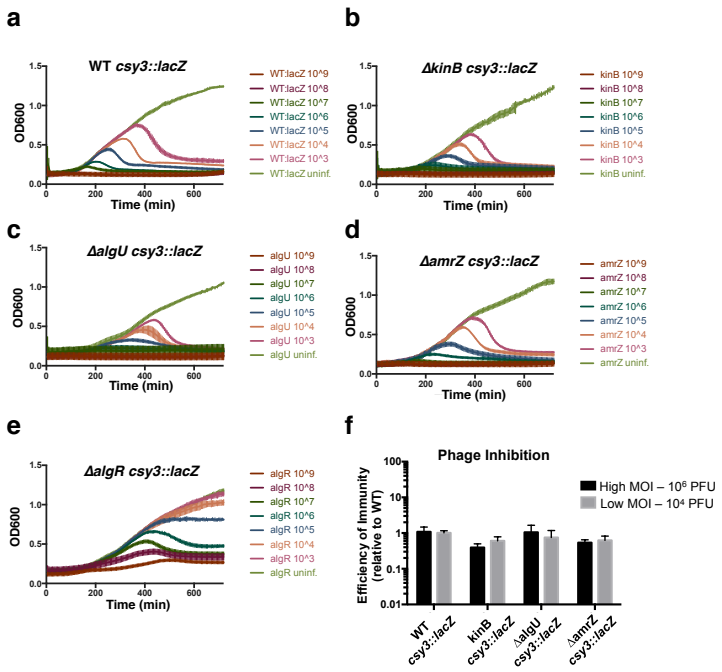

Supplementary Figure 3:

a-e. Growth curves of the indicated knockouts combined with *csy3::lacZ*. infected with virulent DMS3m$_{acrIF4}$ at multiplicity of infection (MOI, rainbow colors) increasing in 10-fold steps from $2x10^{-4}$ to $2x10^{2}$. **f.** Phage replication was quantified as PFUs after 24 hours for the MOIs used in Figure 1 and 3, and the efficiency of immunity expressed as a ratio of the number of PFUs harvested from the mutants combined with *csy3::lacZ* under the number of PFUs obtained from WT *csy::lacZ*. OD600 and EOI measurements are represented as the mean of 3 biological replicates +/- SD.

Supplementary Figure 4

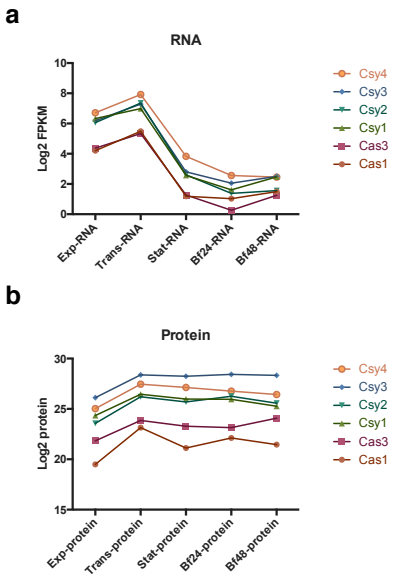

585

586 **Supplementary Figure 4.**

587 **a.** Log2 of Fragments Per Kilobase of transcript per Million mapped reads (FPKM)
588 shown for each I-F *cas* gene in PA14 in the indicated growth condition. **b.** Log2 of
589 protein levels for each of the I-F Cas proteins in PA14 in the indicated growth condition.

590

591

592 **REFERENCES**

593 1. Makarova, K. S. *et al.* An updated evolutionary classification of CRISPR-Cas
594 systems. *Nat Rev Micro* **13,** 722–736 (2015).
595 2. Sapranauskas, R. *et al.* The Streptococcus thermophilus CRISPR/Cas system
596 provides immunity in Escherichia coli. *Nucleic Acids Research* **39,** 9275–9282
597 (2011).
598 3. Vorontsova, D. *et al.* Foreign DNA acquisition by the I-F CRISPR-Cas system
599 requires all components of the interference machinery. *Nucleic Acids Research*
600 **43,** 10848–10860 (2015).
601 4. Mali, P. *et al.* RNA-guided human genome engineering via Cas9. *Science* **339,**
602 823–826 (2013).
603 5. Cong, L. *et al.* Multiplex Genome Engineering Using CRISPR/Cas Systems.
604 *Science* **339,** 819–823 (2013).
605 6. Leon, L. M., Mendoza, S. D. & Bondy-Denomy, J. How bacteria control the
606 CRISPR-Cas arsenal. *Curr Opin Microbiol* **42,** 87–95 (2018).
607 7. Patterson, A. G., Yevstigneyeva, M. S. & Fineran, P. C. Regulation of CRISPR-
608 Cas adaptive immune systems. *Curr Opin Microbiol* **37,** 1–7 (2017).
609 8. Høyland-Kroghsbo, N. M. *et al.* Quorum sensing controls the Pseudomonas
610 aeruginosa CRISPR-Cas adaptive immune system. *Proceedings of the National*
611 *Academy of Sciences* **114,** 201617415–135 (2016).
612 9. Patterson, A. G. *et al.* Quorum Sensing Controls Adaptive Immunity through the

613 Regulation of Multiple CRISPR-Cas Systems. *Mol Cell* **64,** 1102–1108 (2016).
614 10. Høyland-Kroghsbo, N. M., Muñoz, K. A. & Bassler, B. L. Temperature, by
615 Controlling Growth Rate, Regulates CRISPR-Cas Activity in Pseudomonas
616 aeruginosa. *mBio* **9,** 1709–12 (2018).
617 11. Perez-Rodriguez, R. *et al.* Envelope stress is a trigger of CRISPR RNA-mediated
618 DNA silencing in Escherichia coli. *Molecular Microbiology* **79,** 584–599 (2011).
619 12. Serbanescu, M. A. *et al.* Role of the Streptococcus mutans CRISPR/Cas systems
620 in immunity and cell physiology. (2014). doi:10.1128/JB.02333-14
621 13. Shinkai, A. *et al.* Transcription activation mediated by a cyclic AMP receptor
622 protein from Thermus thermophilus HB8. *J. Bacteriol.* **189,** 3891–3901 (2007).
623 14. Patterson, A. G., Chang, J. T., Taylor, C. & Fineran, P. C. Regulation of the Type
624 I-F CRISPR-Cas system by CRP-cAMP and GalM controls spacer acquisition and
625 interference. *Nucleic Acids Research* **43,** gkv517–6048 (2015).
626 15. Agari, Y. *et al.* Transcription profile of Thermus thermophilus CRISPR systems
627 after phage infection. *Journal of Molecular Biology* **395,** 270–281 (2010).
628 16. Young, J. C. *et al.* Phage-induced expression of CRISPR-associated proteins is
629 revealed by shotgun proteomics in Streptococcus thermophilus. *PLoS ONE* **7,**
630 e38077 (2012).
631 17. Quax, T. E. F. *et al.* Massive activation of archaeal defense genes during viral
632 infection. *Journal of Virology* **87,** 8419–8428 (2013).
633 18. Fusco, S. *et al.* Transcriptome analysis of Sulfolobus solfataricus infected with two
634 related fuselloviruses reveals novel insights into the regulation of CRISPR-Cas
635 system. *Biochimie* (2015). doi:10.1016/j.biochi.2015.04.006
636 19. Brouns, S. J. J. *et al.* Small CRISPR RNAs guide antiviral defense in prokaryotes.
637 *Science* **321,** 960–964 (2008).
638 20. Hochstrasser, M. L. *et al.* CasA mediates Cas3-catalyzed target degradation
639 during CRISPR RNA-guided interference. *Proceedings of the National Academy*
640 *of Sciences* **111,** 6618–6623 (2014).
641 21. Westra, E. R. *et al.* CRISPR Immunity Relies on the Consecutive Binding and
642 Degradation of Negatively Supercoiled Invader DNA by Cascade and Cas3. *Mol*
643 *Cell* **46,** 595–605 (2012).
644 22. Levy, A. *et al.* CRISPR adaptation biases explain preference for acquisition of
645 foreign DNA. **520,** 505–510 (2015).
646 23. Cady, K. C., Bondy-Denomy, J., Heussler, G. E., Davidson, A. R. & O'Toole, G. A.
647 The CRISPR/Cas Adaptive Immune System of *Pseudomonas aeruginosa*
648 Mediates Resistance to Naturally Occurring and Engineered Phages. 1–40
649 (2012).
650 24. Haurwitz, R. E., Jinek, M., Wiedenheft, B., Zhou, K. & Doudna, J. A. Sequence-
651 and Structure-Specific RNA Processing by a CRISPR Endonuclease. *Science*
652 **329,** 1355–1358 (2010).
653 25. Wiedenheft, B. *et al.* Structural basis for DNase activity of a conserved protein
654 implicated in CRISPR-mediated genome defense. *Structure* **17,** 904–912 (2009).
655 26. Wiedenheft, B. *et al.* RNA-guided complex from a bacterial immune system
656 enhances target recognition through seed sequence interactions. *Proceedings of*
657 *the National Academy of Sciences* **108,** 10092–10097 (2011).
658 27. Rollins, M. F., Schuman, J. T., Paulus, K., Bukhari, H. S. T. & Wiedenheft, B.
659 Mechanism of foreign DNA recognition by a CRISPR RNA-guided surveillance
660 complex from Pseudomonas aeruginosa. *Nucleic Acids Research* (2015).
661 doi:10.1093/nar/gkv094
662 28. Rollins, M. F. *et al.* Cas1 and the Csy complex are opposing regulators of Cas2/3
663 nuclease activity. *Proceedings of the National Academy of Sciences* **23,**

664 201616395–E5121 (2017).
665 29. Chowdhury, S. *et al.* Structure Reveals Mechanisms of Viral Suppressors that
666 Intercept a CRISPR RNA-Guided Surveillance Complex. *Cell* **169,** 47–57.e11
667 (2017).
668 30. Zegans, M. E. *et al.* Interaction between bacteriophage DMS3 and host CRISPR
669 region inhibits group behaviors of Pseudomonas aeruginosa. *J. Bacteriol.* **191,**
670 210–219 (2009).
671 31. Cady, K. C. & O'Toole, G. A. Non-identity-mediated CRISPR-bacteriophage
672 interaction mediated via the Csy and Cas3 proteins. *J. Bacteriol.* **193,** 3433–3445
673 (2011).
674 32. van Belkum, A. *et al.* Phylogenetic Distribution of CRISPR-Cas Systems in
675 Antibiotic-Resistant Pseudomonas aeruginosa. *mBio* **6,** e01796–15 (2015).
676 33. Westra, E. R. *et al.* Parasite Exposure Drives Selective Evolution of Constitutive
677 versus Inducible Defense. *Curr. Biol.* **25,** 1043–1049 (2015).
678 34. van Houte, S. *et al.* The diversity-generating benefits of a prokaryotic adaptive
679 immune system. *Nature* **532,** 385–388 (2016).
680 35. Bondy-Denomy, J., Pawluk, A., Maxwell, K. L. & Davidson, A. R. Bacteriophage
681 genes that inactivate the CRISPR/Cas bacterial immune system. *Nature* **493,**
682 429–432 (2013).
683 36. Pawluk, A., Bondy-Denomy, J., Cheung, V. H. W., Maxwell, K. L. & Davidson, A.
684 R. A new group of phage anti-CRISPR genes inhibits the type I-E CRISPR-Cas
685 system of Pseudomonas aeruginosa. *mBio* **5,** e00896–e00896–14 (2014).
686 37. Bondy-Denomy, J. *et al.* Multiple mechanisms for CRISPR-Cas inhibition by anti-
687 CRISPR proteins. *Nature* **526,** 136–139 (2015).
688 38. Pawluk, A. *et al.* Inactivation of CRISPR-Cas systems by anti-CRISPR proteins in
689 diverse bacterial species. *Nature Microbiology* **1,** 1–6 (2016).
690 39. Cady, K. C. & O'Toole, G. Non-Identity-Mediated CRISPR-Bacteriophage
691 Interaction Mediated via the Csy and Cas3 Proteins. **193,** 3433–3445 (2011).
692 40. Cady, K. C., Bondy-Denomy, J., Heussler, G. E., Davidson, A. R. & O'Toole, G. A.
693 The CRISPR/Cas adaptive immune system of Pseudomonas aeruginosa
694 mediates resistance to naturally occurring and engineered phages. **194,** 5728–
695 5738 (2012).
696 41. Borges, A. L. *et al.* Bacteriophage Cooperation Suppresses CRISPR-Cas3 and
697 Cas9 Immunity. *Cell* **174,** 917–925.e10 (2018).
698 42. Damron, F. H. *et al.* Analysis of the Pseudomonas aeruginosa Regulon Controlled
699 by the Sensor Kinase KinB and Sigma Factor RpoN. **194,** 1317–1330 (2012).
700 43. Martin, D. W. *et al.* Mechanism of conversion to mucoidy in Pseudomonas
701 aeruginosa infecting cystic fibrosis patients. *Proc Natl Acad Sci USA* **90,** 8377–
702 8381 (1993).
703 44. Qiu, D., Eisinger, V. M., Rowen, D. W. & Yu, H. D. Regulated proteolysis controls
704 mucoid conversion in Pseudomonas aeruginosa. *Proc Natl Acad Sci USA* **104,**
705 8107–8112 (2007).
706 45. Chand, N. S. *et al.* The Sensor Kinase KinB Regulates Virulence in Acute
707 Pseudomonas aeruginosa Infection. **193,** 2989–2999 (2011).
708 46. Chand, N. S., Clatworthy, A. E. & Hung, D. T. The Two-Component Sensor KinB
709 Acts as a Phosphatase To Regulate Pseudomonas aeruginosa Virulence. **194,**
710 6537–6547 (2012).
711 47. Damron, F. H., Qiu, D. & Yu, H. D. The Pseudomonas aeruginosa Sensor Kinase
712 KinB Negatively Controls Alginate Production through AlgW-Dependent MucA
713 Proteolysis. **191,** 2285–2295 (2009).
714 48. Cezairliyan, B. O. & Sauer, R. T. Control of Pseudomonas aeruginosa AlgW

715 protease cleavage of MucA by peptide signals and MucB. *Molecular Microbiology*
716 **72,** 368–379 (2009).
717 49. Schurr, M. J., Yu, H., Martinez-Salazar, J. M., Boucher, J. C. & Deretic, V. Control
718 of AlgU, a member of the sigma E-like family of stress sigma factors, by the
719 negative regulators MucA and MucB and Pseudomonas aeruginosa conversion to
720 mucoidy in cystic fibrosis. *J. Bacteriol.* **178,** 4997–5004 (1996).
721 50. Tart, A. H., Blanks, M. J. & Wozniak, D. J. The AlgT-dependent transcriptional
722 regulator AmrZ (AlgZ) inhibits flagellum biosynthesis in mucoid, nonmotile
723 Pseudomonas aeruginosa cystic fibrosis isolates. *J. Bacteriol.* **188,** 6483–6489
724 (2006).
725 51. Baynham, P. J. & Wozniak, D. J. Identification and characterization of AlgZ, an
726 AlgT-dependent DNA-binding protein required for Pseudomonas aeruginosa algD
727 transcription. *Molecular Microbiology* **22,** 97–108 (1996).
728 52. Wozniak, D. J. & Ohman, D. E. Transcriptional analysis of the Pseudomonas
729 aeruginosa genes algR, algB, and algD reveals a hierarchy of alginate gene
730 expression which is modulated by algT. *J. Bacteriol.* **176,** 6007–6014 (1994).
731 53. Landsberger, M. *et al.* Anti-CRISPR Phages Cooperate to Overcome CRISPR-
732 Cas Immunity. *Cell* **174,** 908–916.e12 (2018).
733 54. Kong, W. *et al.* ChIP-seq reveals the global regulator AlgR mediating cyclic di-
734 GMP synthesis in Pseudomonas aeruginosa. *Nucleic Acids Research* **43,** 8268–
735 8282 (2015).
736 55. Lizewski, S. E. *et al.* Identification of AlgR-regulated genes in Pseudomonas
737 aeruginosa by use of microarray analysis. *J. Bacteriol.* **186,** 5672–5684 (2004).
738 56. Schulz, S. *et al.* Elucidation of sigma factor-associated networks in Pseudomonas
739 aeruginosa reveals a modular architecture with limited and function-specific
740 crosstalk. *PLoS Pathog* **11,** e1004744 (2015).
741 57. Wozniak, D. J. *et al.* Alginate is not a significant component of the extracellular
742 polysaccharide matrix of PA14 and PAO1 Pseudomonas aeruginosa biofilms.
743 *Proc Natl Acad Sci USA* **100,** 7907–7912 (2003).
744 58. Pryor, E. E. *et al.* The transcription factor AmrZ utilizes multiple DNA binding
745 modes to recognize activator and repressor sequences of Pseudomonas
746 aeruginosa virulence genes. *PLoS Pathog* **8,** e1002648 (2012).
747 59. Pratama, A. A. & van Elsas, J. D. A novel inducible prophage from the
748 mycosphere inhabitant Paraburkholderia terrae BS437. *Sci Rep* **7,** 9156 (2017).
749 60. Boucher, J. C., Yu, H., Mudd, M. H. & Deretic, V. Mucoid Pseudomonas
750 aeruginosa in cystic fibrosis: characterization of muc mutations in clinical isolates
751 and analysis of clearance in a mouse model of respiratory infection. *Infection and*
752 *Immunity* **65,** 3838–3846 (1997).
753 61. Martin, D. W., Holloway, B. W. & Deretic, V. Characterization of a locus
754 determining the mucoid status of Pseudomonas aeruginosa: AlgU shows
755 sequence similarities with a Bacillus sigma factor. *J. Bacteriol.* **175,** 1153–1164
756 (1993).
757 62. Damron, F. H., Qiu, D. & Yu, H. D. The Pseudomonas aeruginosa sensor kinase
758 KinB negatively controls alginate production through AlgW-dependent MucA
759 proteolysis. *J. Bacteriol.* **191,** 2285–2295 (2009).
760 63. Jones, A. K. *et al.* Activation of the Pseudomonas aeruginosa AlgU regulon
761 through mucA mutation inhibits cyclic AMP/Vfr signaling. **192,** 5709–5717 (2010).
762 64. Heilmann, S., Sneppen, K. & Krishna, S. Sustainability of virulence in a phage-
763 bacterial ecosystem. *Journal of Virology* **84,** 3016–3022 (2010).
764 65. Dötsch, A. *et al.* The Pseudomonas aeruginosaTranscriptional Landscape Is
765 Shaped by Environmental Heterogeneity and Genetic Variation. *mBio* **6,** e00749–

766 15–10 (2015).
767 66. Erdmann, J., Preusse, M., Khaledi, A., Pich, A. & Häussler, S. Environment-driven
768 changes of mRNA and protein levels in Pseudomonas aeruginosa. *Environmental*
769 *Microbiology* **20,** 3952–3963 (2018).
770